HHS Public Access

Author manuscript

Magn Reson Med. Author manuscript; available in PMC 2018 May 01.

Published in final edited form as:

Magn Reson Med. 2017 May ; 77(5): 2005–2014. doi:10.1002/mrm.26278.

Noninvasive detection of enzyme activity in tumor models of human ovarian cancer using catalyCEST MRI

Sanhita Sinharay, MS[*], **Edward A. Randtke, PhD**[†], **Kyle M. Jones, BS**[‡], **Christine M. Howison, BS**[†], **Setsuko K. Chambers, MD**[§,¶], **Hisataka Kobayashi, MD, PhD**[#], and **Mark D. Pagel, PhD**[*,†,¶]

[*]Department of Chemistry and Biochemistry, University of Arizona, Tucson, AZ

[†]Department of Medical Imaging, University of Arizona, Tucson, AZ

[‡]Biomedical Engineering Graduate Interdisciplinary Program, University of Arizona, Tucson, AZ

[§]Department of Obstetrics and Gynecology, University of Arizona, Tucson, AZ

[¶]University of Arizona Cancer Center, University of Arizona, Tucson, AZ

[#]Laboratory of Molecular Theranostics, National Cancer Institute, NIH

Abstract

Purpose—We proposed to detect the *in vivo* enzyme activity of γ-glutamyl transferase (GGT) within mouse models of human ovarian cancers using catalyCEST MRI with a diamagnetic CEST agent.

Methods—A CEST-FISP MRI protocol and a diamagnetic CEST agent were developed to detect GGT enzyme activity in biochemical solution. A quantitative Michaelis-Menten enzyme kinetics study was performed to confirm that catalyCEST MRI can measure enzyme activity. *In vivo* catalyCEST MRI studies generated pixelwise activity maps of GGT activities. *Ex vivo* fluorescence imaging was performed for validation.

Results—CatalyCEST MRI selectively detected two CEST signals from a single CEST agent, whereby one CEST signal was responsive to GGT enzyme activity and the other CEST signal was an unresponsive control signal. The comparison of these CEST signals facilitated *in vivo*

Corresponding Author: Mark D. Pagel, Ph.D. Vice Chair of Research and Program Development, Director of Cancer Imaigng and Associate Professor, Department of Medical Imaging, University of Arizona, 1515 N. Campbell Ave. Tucson, AZ 85724-5024, Tel: (520)-404-7049, mpagel@u.arizona.edu.

Sanhita Sinharay, M.S., Graduate Research Assistant, Department of Chemistry and Biochemistry, University of Arizona, 1515 N. Campbell Ave. Tucson, AZ 85724-5024

Edward A. Randtke, Ph.D., Research Assistant Professor, Department of Medical Imaging, University of Arizona, 1515 N. Campbell Ave. Tucson, AZ 85724-5024

Christine M. Howison, B.S., Director of Pre-clinical Imaging, Department of Medical Imaging, University of Arizona, 1515 N. Campbell Ave. Tucson, AZ 85724-5024

Kyle M. Jones, B.S., Graduate Research Assistant, Department of Biomedical Engineering, University of Arizona, 1515 N. Campbell Ave. Tucson, AZ 85724-5024

Setsuko K. Chambers, M.D., Bobbi Olsen Endowed Chair in Ovarian Cancer, Department of Obstetrics and Gynecology, University of Arizona, 1501 N. Campbell Ave. Tucson, AZ 85724-5024

Hisataka Kobayashi, M.D., Ph.D., Head, Laboratory of Molecular Theranostics, Center for Cancer Research, National Cancer Institute, Bldg 10, Room B3B47, Bethesda, MD 20892-1088

Conflict of Interest statement: The authors declare no conflicts of interest that pertain to this research.

catalyCEST MRI studies that detected high GGT activity in OVCAR-8 tumors, low GGT activity in OVCAR-3 tumors, and low or no GGT activity in muscle tissues.

Conclusions—CatalyCEST MRI with a diamagnetic CEST agent can detect the level of GGT enzyme activity within *in vivo* tumor models of human ovarian cancers.

Keywords

CEST MRI; enzyme activity; ovarian cancer; molecular imaging; glutamyl transferase

Introduction

The detection of extracellular enzyme activity may potentially improve disease diagnoses relative to only monitoring enzyme expressions. These detections of enzyme activities should occur within the *in vivo* pathological tissue because the level of enzyme activity can be modulated by environmental conditions that are not present during *in vitro* or *ex vivo* studies. For example, γ-glutamyl transferase (GGT) catalyzes the cleavage of a γ-glutamyl moiety of extracellular glutathione (Fig. 1a) in the extracellular space of ovarian, liver, breast, and squamous skin cancers.[1,2,3] The intracellular transport of the cleaved products then reduces oxidative stress that promotes tumor cell survival and division, tumor progression, and resistance to platinum-containing chemotherapies.[4] Elevated GGT activity is associated with increased risk of ovarian, breast, prostate, and liver cancers. Therefore, a non-invasive imaging method could be useful for interrogating GGT activity to diagnose tumor stage, prognosticate survival, and predict response to some types of chemotherapies.[5]

As another potential application, the activity of GGT has been detected during optical surgical navigation to improve the localization of proliferating, metastatic tumors during surgery.[6,7] This detection relies on a substrate that becomes fluorescent after GGT cleaves a glutamyl ligand from a rhodamine-based dye (Fig. 1b). However, only a subset of tumors have active GGT enzyme.[7] A complimentary imaging method that non-invasively detects GGT activity is needed to pre-screen patients prior to surgery, to select patients who are candidates for optical surgical navigation.

Chemical Exchange Saturation Transfer (CEST) MRI involves saturation of the magnetization of a specific proton in a contrast agent (Fig. 2a, first step).[8] The subsequent transfer of the saturated proton to a bulk water molecule via chemical exchange (Fig. 2a, second step) decreases the MRI signal of the water that can be detected with a standard MRI protocol. CatalyCEST MRI detects a change in a CEST signal after enzyme catalysis, and then compares the detection of enzyme-responsive CEST signal with an enzyme-unresponsive control CEST signal (Fig. 2b).[9] To date, CEST MRI contrast agents have been developed that detect the enzyme activity of proteases, esterases, a kinase, deaminase, galactosidase, and transglutaminase, although most of these agents lack an enzyme-unresponsive CEST signal.[9–19] Furthermore, most catalyCEST MRI studies have used paramagnetic agents with metallic ions that are potentially toxic, which hampers clinical translation.[20]

To overcome hurdles for clinical translation of catalyCEST MRI, we sought to develop a single CEST agent that is nonmetallic, has enzyme-responsive and unresponsive CEST signals, and can detect the enzyme activity of GGT within *in vivo* tumor tissues (Fig. 1c, 2b).[21] Our agent was designed by adding a glutamyl ligand to salicylic acid.[22,23] We investigated the synthesis and biochemical characterization of the agent, including Michaelis-Menten enzyme kinetics studies to investigate the catalytic cleavage of the agent by GGT. We then performed *in vivo* catalyCEST MRI studies with mouse models of OVCAR-8 and OVCAR-3 human ovarian cancer as well as muscle, which have high, low, and no GGT activity, respectively. Finally, we compared our catalyCEST MRI studies with results from *ex vivo* fluorescence imaging studies.

Materials and Methods

Initial catalyCEST MRI studies

The chemical synthesis of the agent is described in the Supporting Information. The agent was prepared at 25 mM concentration in PBS buffer (5x strength, pH 7.2). Samples were placed in a sample holder that maintained the samples at 37.00.2 °C. To identify the location of the samples in the magnet, an initial set of images were acquired using a multislice spin echo MRI protocol with the following parameters TR: 500 ms; TE: 10.0 ms; excitation flip angle: 90°; matrix: 128 ×128; field of view: 8×8 cm; in-plane spatial resolution: 625×625 μm; slice thickness: 1 mm; number of slices: 30; number of averages: 1; total scan time: 1:04 min.

We used a CEST-FISP MRI acquisition protocol with the following parameters TR: 3.196 ms; TE: 1.598 ms; excitation flip angle: 30°; centric encoding during acquisition; matrix: 128×128; field of view: 8×8 cm; in-plane spatial resolution: 625×625 μm; slice thickness: 1 mm; number of slices: 1; number of averages: 1.[24] We acquired a series of 85 images with selective saturation applied at 3 μT for 5 seconds at saturation frequencies in 0.25 ppm increments from 15 ppm to −3 ppm and 1 ppm increments from −4 ppm to −15 ppm, for a total scan time of 7:42 min. MRI studies were performed with a Biospec MRI scanner operating at 7 T (300 MHz) magnetic field strength with a 72 mm volume transceiver coil (Bruker Biospin, Inc., Billerica, MA). Then 0.4 units of GGT enzyme were added to a 200 μL, 25 mM solution of the contrast agent. The solution was incubated for 12 h at 37°C. The same CEST-FISP MRI protocol was then used to obtain CEST spectra after GGT enzyme catalysis.

Images were processed using ParaVision v5.1, and CEST MR image analyses were performed with Matlab v8.4 (Mathworks, Natick, MA). To measure CEST signal amplitudes, each CEST spectrum from a region of interest (ROI) in an image of a sample was analyzed by fitting the spectrum to a sum of three Lorentzian line shapes to account for two CEST signals and direct saturation of water.[18] The center, width, and amplitude of each Lorentzian line was allowed to change to optimize the fit.

Optimization of the catalyCEST MRI protocol

CEST spectra were acquired with a 25 mM solution of the agent in PBS buffer at pH 7.3 using the same CEST-FISP MRI protocol at saturation powers ranging from 1 μT to 7 μT and using a saturation time of 5 s. A HW-QUESP analysis method was used to determine the chemical exchange rates of the reactant and product.[25] This linear analysis method has been shown to more accurately measure chemical exchange rates relative to the non-linear QUESP analysis method or the linear LB-QUESP method (also known as the Omega plot method). CEST spectra were obtained at saturation times ranging from 0.2 s to 12 s using the same sample and with a saturation power of 3 μT. Although subsequent analyses indicated that a saturation power higher than 3 μT can produce stronger CEST signals, the 3 μT saturation power was sufficient for optimizing other parameters of the catalyCEST MRI protocol. A RL-QUEST plot was used to assess the optimal saturation time for subsequent experiments.[26] To study the effect of pH on both CEST signals, 25 mM samples of the agent were prepared with pH values ranging from 6.2 to 7.4 and CEST spectra were collected with a saturation power of 3 μT and a saturation time of 5 s. Finally, CEST MRI was performed with samples of the agent ranging from 10 mM to 75 mM, and with a saturation pulse of 3 μT and 5 s saturation time. A HW-Conc analysis method was used to calibrate CEST signal with concentration, which was useful for Michaelis-Menten kinetics analysis.[27]

Michaelis-Menten enzyme kinetics studies with catalyCEST MRI

The kinetics of the cleavage of the agent by GGT was studied using catalyCEST MRI with the same CEST-FISP MRI protocol using a saturation pulse of 3 μT and 5 s saturation time. Samples of the agent ranging in concentration from 3.5 to 68 mM were prepared in PBS 5x buffer to maintain a pH between 7.35 and 7.4 units, in a final volume of 200 μL. Then 0.2 units of GGT were added to each sample of the agent, and 80 CEST spectra were repetitively acquired during 10 hours. The initial velocity of each reaction, v_0, was determined from the first 2.5 hours of the reaction. A Hanes-Woolf plot was used to determine the Michaelis constant, K_m, and the reaction velocity, V_{max}.[28] The catalysis rate, k_{cat}, was determined from V_{max} and the initial enzyme concentration. The catalytic efficiency, k_{cat}/K_M, was then determined from these results.

In vivo catalyCEST MRI studies

All *in vivo* studies were approved by the Institutional Animal Care and Use Committee of the University of Arizona. To prepare the mouse models of human ovarian cancer, female mice that were 6 to 8 weeks in age were injected with 1×10^6 to 2×10^6 tumor cells suspended in 200 μL to 300 μL of PBS in female nude mice. Both OVCAR-8 and OVCAR-3 human ovarian cancer cells were used for this study. Imaging studies were performed 25 days post injection for the OVCAR-8 tumor model and 40 days for the OVCAR-3 tumor model, when the tumor reached approximately 300 mm^3 in diameter.

CatalyCEST MRI was performed using two mice with an orthotopic OVCAR-8 tumor, two mice with orthotopic OVCAR-3 tumor, and two mice to study enzyme activity in muscle tissue. Each mouse was anesthetized with 1.5–2.5% isoflurane delivered in 1 L/min oxygen gas ventilation. The mouse was then secured to a customized MRI–compatible cradle, probes for monitoring rectal temperature and respiration were connected to the mouse, and

core body temperature was regulated at 37.0 ± 0.2°C using an air heater (SA instruments, Inc., Stony Brook, NY). To identify the location of the tumor or muscle tissue, an initial set of images were acquired using a multislice spin echo MRI protocol with the following parameters TR: 1200 ms; TE: 21.26 ms; excitation flip angle: 90°; matrix: 256×128; field of view: 6×4 cm; in-plane spatial resolution: 234×312 μm; slice thickness: 1 mm; number of slices: 17; number of averages: 1; total scan time: 2:33 min. After identifying the tumor or muscle location with MRI, the mouse was temporarily removed from the magnet, a solution of 500 mM of the agent in 250 μL was injected into the mouse intraperitoneally within 5 mm of the tumor or was injected intramuscularly, the mouse was reinserted into the magnet, and a 10-minute delay occurred before imaging to allow the agent to be cleaved by GGT. The *in vivo* CEST-FISP MRI studies used the following parameters of TR: 3.698 ms; TE: 1.649 ms; excitation flip angle: 15°; with radiofrequency spoiling; centric encoding during acquisition; matrix: 128 ×128; field of view: 6×4 cm; in-plane spatial resolution: 469×312 μm; slice thickness: 2 mm; number of slices: 1; number of averages: 1. Ten 600 ms continuous wave saturation pulses at a saturation power of 4 μT were used at each saturation frequency. Respiration gating was used to reduce motion artifacts (Fig. 3).[29] A series of nine catalyCEST MRI scans were acquired with a series of 41 saturation frequencies at ppm values of +14, +13, +12.6 to 3 (with 0.4 ppm increments), +2.5 to −2.0 (with 0.5 ppm increments), and −3 to −12 (with 3 ppm increments). The total scan time for one CEST spectrum was 4:24 to 4:48 min depending on the timing of respiration gating. Nine consecutive CEST spectra were acquired. At the conclusion of the MR scan, the mouse was removed from the magnet and cradle and allowed to recover.

To obtain parametric maps of the CEST signal amplitudes during *in vivo* catalyCEST MRI studies, the images from the nine repetitions were averaged, and a Gaussian spatial filter was applied to the average image with a 3×3 pixel matrix and a σ value of one pixel.[30] The ROI for the tumor or muscle tissue was determined from the anatomical MR images. The CEST spectrum from each pixel in the image was obtained from the MR images. Linear baseline correction was applied to account for power drift of the gradient amplifier, and possible heating of the static shim coils or sample. A function of four Lorentzian line shapes was fit to each CEST spectrum to measure the signal amplitudes of the CEST effects at 4.8 and 9.2 ppm, and also account for direct saturation of water and the endogenous effect of amide proton transfer.[19] The saturation frequency, width and amplitude of the Lorentzian line shape that fit the direct saturation of water was allowed to change during the fitting procedure. The width and amplitude of the two Lorentzian line shapes that fit the CEST effects of the agent were also allowed to change, but the saturation frequencies of these Lorentzian line shapes were fixed at 9.2 and 4.8 ppm relative to the saturation frequency of the direct saturation of water. The parametric maps of the reaction coordinates of GGT enzyme activity were determined using Eq. [1]. CEST spectra were obtained for the ROI of each tumor and muscle tissue by averaging the images, applying a Gaussian spatial filter, linear baseline fitting to account for power drift of the gradient amplifier, and averaging the CEST spectra of the pixels in the ROI. The same Lorentzian line shape fitting method was applied to each of these CEST spectra of each ROI.

$$RC = 1 - \frac{CEST\ signal\ amplitude\ at\ 4.8ppm}{CEST\ signal\ amplitude\ at\ 9.2ppm} \quad \text{Eq. [1]}$$

The temporal change in CEST was evaluated during the *in vivo* enzyme activity study of the OVCAR-8 tumor model. The CEST spectra of the ROI that represented the tumor were obtained for each of the nine time points. The CEST spectra of time points 1–3, 2–4, 3–5, 4–6, 5–7, 6–8, and 7–9 were each averaged to generate results at 7 time points, and Lorentzian line fitting was performed to measure the two CEST signal amplitudes. The ratio of the CEST signal amplitude at 4.8 ppm vs. the CEST signal amplitude at 9.2 ppm was then fit to a function with a single exponential decay with a constant, because the enzyme catalysis is a pseudo-first order kinetics reaction.

Ex vivo fluorescence imaging studies

Fluorescence imaging studies were performed 24 h after catalyCEST MRI studies. A 250 μL solution of 100 μM of the gGlu-HMRG probe was intraperitoneally injected into the mouse.[6] After 10 minutes, the mouse was euthanized and the abdominal cavity was exposed, which required 5 minutes for preparation. A fluorescence image was collected using an AMI-X imaging system (Spectral Instruments Imaging, Inc, Tucson, AZ) using a 5 s exposure time and excitation and emission filters at 490 and 550 nm, respectively. Additional images were collected at 10, 20 and 30 minutes after the initial image was acquired. All four images showed identical fluorescence signal amplitude, which indicated that the timing of the image acquisition was not critical.

Results

Development of the GGT-responsive catalyCEST MRI contrast agent

We synthesized the CEST agent, 4-amino salicylic acid with a glutamyl moiety (**4**), with an overall yield of 47% (Sup. Fig. S1). A CEST-FISP MRI protocol was used to obtain a CEST spectrum of this agent (Fig. 2c).[24] This agent generated a CEST signal at 9.2 ppm from the salicylic acid moiety and a second CEST signal at 4.8 ppm from the aryl amide moiety. The ppm values of these CEST signals were similar to the CEST signal from agents that have a single salicylic acid moiety or a single aryl amide moiety.[22,23,31] Therefore, the two CEST signals from this single agent did not overlap, and were substantially different from the chemical shift of water, which greatly facilitated the detection and analysis of each CEST signal.

After adding GGT enzyme, the contrast agent was cleaved to form 4-amino salicylic acid as verified using mass spectrometry. CEST spectra of the product showed that the CEST signal at 4.8 ppm disappeared as a result of GGT cleavage of the glutamyl ligand from the agent, while the CEST signal at 9.2 ppm was largely unchanged (Fig. 2c). This result confirmed that a single diamagnetic CEST agent can generate enzyme-responsive and unresponsive CEST signals, so that the ratio of these signals can be used to detect enzyme activity in a concentration-independent manner.

Optimization of the CEST MRI protocol

We established a CEST MRI protocol that can detect the agent with the best sensitivity. A saturation power of 4 μT (Sup. Fig. S2) was shown to generate relatively strong CEST signals while still maintaining an acceptably low power below the SAR limit for *in vivo* studies, A saturation time of 3 seconds was also adequate for generating strong CEST signals (Sup. Fig. S3).[25,26] In addition, a calibration of CEST signal amplitude vs. concentration was generated using the HW-Conc CEST method to facilitate the kinetics analyses (Sup. Fig. S4).[27]

We used the HW-QUESP CEST MRI method to measure the chemical exchange rate of the salicylic acid proton before and after GGT catalysis and after catalysis. These exchange rates were 848 Hz and 934 Hz, respectively, demonstrating that the chemical exchange of the salicylic acid was largely unaffected by the GGT enzyme activity (Sup. Figs. S2d,f).[25] This result further confirmed that the agent met our requirements for GGT detection with a single, nonmetallic CEST agent with enzyme-responsive and unresponsive CEST signals.

Michaelis-Menten enzyme kinetics studies

To perform Michaelis-Menten enzyme kinetics studies,[10] samples of the agent ranging in concentration from 3.5 to 68 mM were treated with 0.2 units of GGT. A very low concentration of enzyme was used to lengthen the time of the study, which improved the accuracy of the kinetics analysis. Immediately after adding the enzyme, 80 CEST spectra were acquired during 10 hours (Fig. 4a). The amplitude of the CEST signal at 4.8 ppm was converted to concentration of the uncleaved agent at each time point of the reaction, using our previously determined CEST-concentration calibration with an identical CEST MRI protocol. The initial velocity of each reaction, v_0, was determined from the rate of decrease of the uncleaved agent's concentration during the first 2.5 hours of the reaction (Fig. 4b). Although a Lineweaver-Burke plot is often used for enzyme kinetics analysis, a Hanes-Woolf plot was preferred for our study because this analysis method is less sensitive to inaccuracies when measuring substrate concentrations (Fig. 4c).[32] The good fitting of the Hanes-Woolf plot to the experimental results demonstrated that the CEST agent followed Michaelis-Menten kinetics and therefore was responsive to enzyme activity.

The k_{cat} value for the CEST agent was comparable to k_{cat} of a fluorescence substrate with only a 2-fold decrease in this rate for the CEST agent.[6] The Michaelis constant, K_M, for the CEST agent was 550-fold higher than for the fluorescent substrate, demonstrating weaker binding of the CEST agent to the enzyme. The combination of these effects resulted in a 1,170-fold lower catalytic efficiency, k_{cat}/K_M, relative to the fluorescent substrate. This slower catalytic efficiency raised concerns that GGT may not cleave a sufficient amount of the CEST agent during the time frame of *in vivo* studies, which warranted our *in vivo* investigations.

In vivo catalyCEST MRI: Experimental Conditions

To perform *in vivo* catalyCEST MRI studies, we prepared orthotopic models of OVCAR-8 and OVCAR-3 human ovarian cancer that modeled metastatic ovarian cancer in the peritoneal cavity. After acquiring MR images to locate the tumor within the peritoneal

cavity, 250 μL of a 500 mM solution of the contrast agent was administered i.p. near the tumor. In an additional study, the same injection volume at the same concentration was administered in thigh muscle. We developed a respiration-gated CEST-FISP MRI protocol to reduce motion artifacts while imaging tumors in the peritoneal cavity, which was a critical technological innovation that was required to produce high-quality images for CEST MRI studies (Fig. 3).[29] We used this respiration-gated protocol to acquire CEST-FISP MR images for a total time of 31.5 min, which is a reasonable time frame for eventual clinical translation of this method.

In vivo catalyCEST MRI: OVCAR-8 model

Our first study used an OVCAR-8 tumor model that is known to have high GGT expression (Fig. 5, top row).[6] We observed an average of 4.7% CEST signal at 9.2 ppm throughout the tumor region in the CEST MRI image, demonstrating sufficient delivery of the agent into the tumor for CEST MRI detection. We also observed a weaker 1.9% CEST signal at 4.8 ppm, suggesting rapid cleavage of the agent by GGT. We also analyzed the regions surrounding the tumor tissue, including the region where the bolus of agent was detected. We used CEST MR image processing methods to generate parametric maps of the CEST signal amplitudes at 9.2 and 4.8 ppm, which showed some spatial heterogeneity in each signal amplitude throughout the tumor. Despite this heterogeneity, the CEST signal amplitude at 9.2 ppm was higher than the amplitude at 4.8 ppm throughout the entire tumor region. A ratio of these two parametric maps of CEST signal amplitudes were used to generate a GGT activity map, which represented a quantitative assessment of the enzyme reaction coordinate within the *in vivo* tissue. This activity map showed high GGT activity throughout a large majority of the tumor region.

The successful detection of GGT activity with our catalyCEST MRI protocol obviated concerns that the catalytic efficiency of GGT for cleaving the CEST agent would be too slow for *in vivo* studies. To explain this result, we realized that the high concentration of agent needed for CEST MRI detection (relative to the concentration of agent needed for fluorescence imaging) likely causes the GGT enzyme to be saturated with agent, which causes the catalytic rate to approach k_{cat}. As shown in Figure 4d, the k_{cat} values are comparable for GGT cleavage of the CEST agent and fluorescence agent. Therefore, *in vivo* catalyCEST MRI under conditions that saturate the enzyme with agent are a good match with fluorescence imaging studies.

The temporal evolution of the CEST signal amplitudes in the OVCAR-8 tumor region was evaluated to assess the temporal pharmacokinetic wash-out of the agent relative to the temporal effects of enzyme activity (Fig. 6a). Both CEST signals decreased over time, indicating that the agent was slowly cleared from the tumor tissue during the time course of the *in vivo* imaging study. Yet the ratio of the CEST signal amplitudes showed that the CEST signal at 4.8 ppm decreased more rapidly than the signal at 9.2 ppm (Fig. 6b). An enzyme-catalyzed reaction with a substrate concentration that is much higher than the enzyme concentration is a pseudo-first order kinetics process that follows a single-exponential decay. Therefore, we fit the decreasing ratio of CEST signals to a single-exponential function, which demonstrated a qualitative yet reasonable pseudo-first order

kinetics process. This result demonstrated that two CEST signals are critically needed to detect enzyme activity and also account for pharmacokinetics of the agent during *in vivo* studies.

In vivo catalyCEST MRI: OVCAR-3 model

For comparison, our second study used an OVCAR-3 tumor model with low GGT expression (Fig. 5, middle row).[6] Both CEST signals were sufficiently strong for CEST MRI detection, again demonstrating good delivery of the agent to the tumor. The average amplitudes of these two CEST signals were relatively equivalent at 13.1% and 11.2% CEST at 9.2 and 4.8 ppm, respectively, indicating low enzyme activity. The parametric maps of the two CEST signal amplitudes showed uniform signal amplitudes throughout the tumor region. The reaction coordinate map of this tumor region demonstrated relatively low GGT activity in this tumor model.

In vivo catalyCEST MRI: muscle tissue

We also performed a third study to measure GGT activity in muscle, after directly injecting the same amount of agent into *in vivo* muscle tissue (Fig. 5, bottom row). Both CEST signals had strong 11.5% average amplitudes, which demonstrated good retention of the agent within the tissue. The equal CEST signal amplitudes indicated a lack of GGT activity. The parametric maps of CEST signal amplitudes and the activity map were each very uniform in muscle tissue.

In vivo catalyCEST MRI: validation studies

To validate these results, we then repeated these three studies with a second set of mice with OVCAR-8 and OVCAR-3 orthotopic tumors, and with muscle tissue. This reproducibility trial generated very similar results that confirmed our initial results (Sup. Fig. S5). We also analyzed regions surrounding the tumor tissue and muscle, including the region where the bolus injection delivered agent. We did not detect CEST signals at 9.2 or 4.8 ppm in regions surrounding the tumor (Sup. Fig. S6), suggesting that the agent may have faster pharmacokinetic washout in the peritoneal cavity than the tumor. CEST signals were not detected in regions surrounding the muscle tissue where the agent was injected.

pH and catalyCEST MRI

We evaluated the effect of pH on CEST signal amplitudes (Fig. 7a). The salicylic acid and aryl amide protons both generated higher CEST signal amplitudes at higher pH values, which was expected due to the base-catalyzed chemical exchange mechanism for these two moieties.[22,31] Both CEST signal amplitudes are equal at pH 7.4, and the CEST signal amplitude of salicylic acid is less than the CEST signal of the amide proton at lower pH. Therefore, the reaction coordinate of GGT activity is underestimated at lower pH (Fig. 7b). Tumor tissues can be acidic,[33,34] which raises concerns that the reaction coordinate values are underestimated in the enzyme activity maps of the tumors. Yet our results show that the enzyme activity is high in the OVCAR-8 tumor relative to muscle, so correcting for this underestimation in tumor tissue would only serve to improve this result. Furthermore, we estimate that the OVCAR-3 tumor model would need to be lower in extracellular pH by

more than 1.2 pH units relative to the OVCAR-8 tumor model to account for the differences in reaction coordinates observed in the activity maps of Figure 4 and Supplemental Figure S6. This difference in extracellular pH between these tumor types is unrealistic.

Ex vivo validation

We performed fluorescence imaging studies soon after our MRI studies to validate GGT expression. We administered gGlu-HMRG dye i.p. to each mouse model of metastasized OVCAR-8 or OVCAR-3 ovarian cancers.[6] Each mouse was sacrificed ten minutes after administration, and the abdominal cavity was exposed under a whole-body luminescence imaging system (Fig. 8, Sup. Fig. S7). The tumor location and size observed with *in vivo* MRI matched the location and size observed with *ex vivo* fluorescence imaging. The activated dye was clearly observed in the peritoneal OVCAR-8 tumor, which confirmed high GGT activity. Only low fluorescence was observed in the OVCAR-3 tumor, and no fluorescence was detected in exposed muscle tissues or other surrounding tissues in either mouse model. Therefore, the fluorescence imaging results matched the catalyCEST MRI results, which provided supporting evidence that catalyCEST MRI detected GGT enzyme activity.

Discussion

Our study has demonstrated the detection of enzyme activity with a single diamagnetic CEST agent that has enzyme-responsive and unresponsive CEST signals. The comparison of both CEST signals was critical to ensuring the detection of enzyme activity while also accounting for pharmacokinetics of the agent during *in vivo* studies. Without the enzyme-unresponsive signal from the salicylic acid moiety, the pharmacokinetic washout of the agent from the tumor that caused a loss of CEST signal from the enzyme-responsive amide group could be misinterpreted as arising from enzyme activity (Fig. 6). Moreover, the absence of the amide's CEST signal from regions surrounding the tumor or muscle could also be misinterpreted as arising from enzyme activity if a CEST signal from salicylic acid was not also incorporated into the experimental design.

Many conditions can influence CEST signals, yet our methodology mitigated or eliminated many conditions that may influence our detection of enzyme activity. Fitting Lorentzian line shapes to CEST spectra compensates for B_0 inhomogeneity;[30] the ratio of two CEST signals eliminates the effect of concentration, endogenous T_1 relaxation time, and B_1 inhomogeneity;[35] multiple pools of exchangeable protons on exogenous contrast agents can be treated independently;[36] the ratio of CEST signals can reduce or eliminate the influence of endogenous exchangeable proton pools;[27] and changes in temperature have negligible influence on the CEST signal ratio within a physiological temperature range.[18] However, as shown in Figure 7, the ratio of CEST signals from this GGT-responsive agent is dependent on pH. Future *in vivo* catalyCEST MRI studies should investigate the effects of tissue pH to improve the detection of enzyme detection. A method known as acidoCEST MRI can produce parametric maps of the extracellular pH values in tumor tissues.[30] Future studies may incorporate acidoCEST MRI methods within catalyCEST MRI studies to correct this pH-dependent underestimation in enzyme reaction coordinate.

Significant *in vivo* enzyme activity was still detected in the OVCAR-3 mouse model with catalyCEST MRI while no activity was detected in the same mice with *ex vivo* fluorescence imaging. This result may suggest that enzymes other than GGT in the OVCAR-3 model cleaved some of the CEST agent that was administered at high concentration, whereby these other enzyme could cleave substrate at their V_{max} rate even if they have a poor K_M constant. Indeed, proteases are notoriously promiscuous and cleave many substrates, so that a single diamagnetic CEST agent substrate may be cleaved by multiple proteases. This enzyme promiscuity has been difficult to study *in vivo* due to a lack of an adequate analysis method. The further development of *in vivo* catalyCEST MRI has good potential to provide a method for *in vivo* assessments of enzyme promiscuity.

The development of a diamagnetic CEST agent for catalyCEST MRI may facilitate translation of this method to the radiology clinic. Paramagnetic CEST agents can only be administered at low doses of approximately 0.1–0.4 mmol/kg mouse body weight, due to concerns regarding toxicity. Diamagnetic CEST agents based on salicylic acid have potentially lower toxicity, providing the opportunity to administer more agent. In our study, we administered 5 mmol/kg of the agent i.p., which showed no evidence for toxicity. Furthermore, our *in vivo* MRI study used a saturation power of 4 μT and a magnetic field strength of 7 T, which have both been used for clinical CEST MRI studies. Finally, our catalyCEST MRI studies were performed in 31.5 min, and may potentially be shortened to further facilitate clinical translation. For these reasons, additional *in vivo* catalyCEST MRI studies with a diamagnetic CEST agent appear warranted to prepare for eventual clinical translation of this method.

Supplementary Material

Refer to Web version on PubMed Central for supplementary material.

Acknowledgments

The authors thank Brenda Baggett and the Experimental Mouse Shared Resource of the University of Arizona Cancer Center for technical assistance through NIH grant P30 CA023074. We also thank Dr. Josef Vagner and Renata Patek for assistance with HPLC purifications. The Phoenix Friends of the Arizona Cancer Center, the Better Than Ever Program, and NIH grant R01CA169774 provided financial support (M.D.P.). K.M.J. is supported by a fellowship from NIH grants T32HL007955 and T32HL066988.

References

1. Hanigan MH, Gallagher BC, Taylor PT, Large MK. Inhibition of γ-glutamyl transpeptidase activity by acivicin in vivo protects the kidney from cisplatin-induced toxicity. Cancer Res. 1994; 54:5925–5929. [PubMed: 7954424]
2. Yao D, Jiang D, Huang Z, Lu J, Tao Q, Yu Z, Meng X. Abnormal expression of hepatoma specific γ-glutamyl transferase and alteration of γ-glutamyl transferase gene methylation status in patients with hepatocellular carcinoma. Cancer. 2000; 88:761–769. [PubMed: 10679644]
3. Grimm C, Hofstetter G, Aust S, Mutz-Dehbalaie I, Bruch M, Heinze G, Rahhal-Schull J, Reinthaller A, Concin N, Polterauer S. Association of gamma-glutamyltransferase with severity of disease at diagnosis and prognosis of ovarian cancer. Brit J Cancer. 2013; 109:610–614. [PubMed: 23921280]
4. Black SM, Wolf CR. The role of glutathione-dependent enzymes in drug resistance. Pharmac Ther. 1991; 51:139–154.

5. Fentiman IS. Gamma-glutamyl transferase: risk and prognosis of cancer. Brit J Cancer. 2012; 106:1467–1468. [PubMed: 22531718]
6. Urano Y, Sakabe M, Kosaka N, et al. Rapid cancer detection by topically spraying a γ-glutamyltranspeptidase–activated fluorescent probe. Sci Transl Med. 2011; 3:110ra119–110ra119.
7. Ueo H, Shinden Y, Tobo T, et al. Rapid intraoperative visualization of breast lesions with γ-glutamyl hydroxymethyl rhodamine green. Sci Rep. 2015; 5:12080. [PubMed: 26165706]
8. Sherry AD, Woods M. Chemical exchange saturation transfer contrast agents for magnetic resonance imaging. Annu Rev Biomed Eng. 2008; 10:391–411. [PubMed: 18647117]
9. Yoo B, Pagel MD. A PARACEST MRI contrast agent to detect enzyme activity. J Am Chem Soc. 2006; 128:14032–14033. [PubMed: 17061878]
10. Yoo B, Raam MS, Rosenblum RM, Pagel MD. Enzyme-responsive PARACEST MRI contrast agents: a new biomedical imaging approach for studies of the proteasome. Contrast Media Mol I. 2007; 2:189–198.
11. Li Y, Sheth VR, Liu G, Pagel MD. A self-calibrating PARACEST MRI contrast agent that detects esterase enzyme activity. Contrast Media Mol I. 2011; 6:219–228.
12. Yoo B, Sheth VR, Pagel MD. An amine-derivatized, DOTA-loaded polymeric support for Fmoc solid phase peptide synthesis. Tet Lett. 2009; 50:4459–4462.
13. Suchý M, Ta R, Li AX, Wojciechowski F, Pasternak SH, Bartha R, Hudson RH. A paramagnetic chemical exchange-based MRI probe metabolized by cathepsin D: design, synthesis and cellular uptake studies. Org Biomolec Chem. 2010; 8:2560–2566. 2010.
14. Hingorani DV, Randtke EA, Pagel MD. A catalyCEST MRI contrast agent that detects the enzyme-catalyzed creation of a covalent bond. J Am Chem Soc. 2013; 135:6396–6398. [PubMed: 23601132]
15. Chauvin T, Durand P, Bernier M, Meudal H, Doan BT, Noury F, Badet B, Beloeil JC, Tóth É. Detection of enzymatic activity by PARACEST MRI: a general approach to target a large variety of enzymes. Angew Chem Int Ed. 2008; 47:4370–4372.
16. Airan RD, Bar-Shir A, Liu G, Pelled G, McMahon MT, van Zijl P, Bulte JW, Gilad AA. MRI biosensor for protein kinase A encoded by a single synthetic gene. Magn Reson Med. 2012; 68:1919–1923. [PubMed: 23023588]
17. Liu G, Liang Y, Bar-Shir A, Chan KW, Galpoththawela CS, Bernard SM, Tse T, Yadav NN, Walczak P, McMahon MT, Bulte JW. Monitoring enzyme activity using a diamagnetic chemical exchange saturation transfer magnetic resonance imaging contrast agent. J Am Chem Soc. 2011; 133:16326–16329. [PubMed: 21919523]
18. Hingorani DV, Montano LA, Randtke EA, Lee YS, Cárdenas-Rodríguez J, Pagel MD. A single diamagnetic catalyCEST MRI contrast agent that detects cathepsin B enzyme activity by using a ratio of two CEST signals. Contrast Media Mol I. 2015; 2015. doi: 10.1002/cmmi.1672
19. Yoo B, Sheth VR, Howison CM, Douglas MJK, Pineda CT, Maine EA, Baker AF, Pagel MD. Detection of in vivo enzyme activity with catalyCEST MRI. Magn Reson Med. 2014; 71:1221–1230. [PubMed: 23640714]
20. Kuo PH, Kanal E, Abu-Alfa AK, Cowper SE. Gadolinium-based MR contrast agents and nephrogenic systemic fibrosis. Radiology. 2007; 242:647–649. [PubMed: 17213364]
21. Nakajima M, Watanabe B, Han L, Shimizu B, Wada K, Fukuyama K, Suzuki H, Hiratake J. Glutathione-analogous peptidyl phosphorus esters as mechanism-based inhibitors of γ-glutamyl transpeptidase for probing cysteinyl-glycine binding site. Bioorg Med Chem. 2014; 22:1176–1194. [PubMed: 24411479]
22. Yang X, Song X, Li Y, Liu G, Ray Banerjee S, Pomper MG, McMahon MT. Salicylic Acid and analogues as diaCEST MRI contrast agents with highly shifted exchangeable proton frequencies. Angew Chem Int Ed. 2011; 52:8116–8119.
23. Song X, Yang X, Ray Banerjee S, Pomper MG, McMahon MT. Anthranilic acid analogs as diamagnetic CEST MRI contrast agents that feature an intramolecular-bond shifted hydrogen. Contrast Media Mol I. 2015; 10:74–80.
24. Shah T, Lu L, Dell KM, Pagel MD, Griswold M, Flask CF. CEST-FISP: A novel technique for rapid chemical exchange saturation transfer MRI at 7 T. Magn Reson Med. 2011; 65:432–437. [PubMed: 20939092]

25. Randtke EA, Chen LQ, Corrales LR, Pagel MD. The Hanes-Woolf linear QUESP method improves the measurements of fast chemical exchange rates with CEST MRI. Magn Reson Med. 2014; 71:1603–1612. [PubMed: 23780911]
26. Randtke EA, Chen LQ, Pagel MD. The reciprocal linear QUEST analysis method facilitates the measurements of chemical exchange rates with CEST MRI. Contrast Media Mol I. 2014; 9:252–258.
27. Ali MM, Liu G, Shah T, Flask CA, Pagel MD. Using two chemical exchange saturation transfer magnetic resonance imaging contrast agents for molecular imaging studies. Accounts Chem Res. 2009; 42:915–924.
28. Hanes CS. Studies on plant amylases: The effect of starch concentration upon the velocity of hydrolysis by the amylase of germinated barley. Biochemical J. 1932; 26:1406–1421.
29. Jones KM, Randtke EA, Howison CM, Cárdenas-Rodríguez J, Sime PJ, Kottmann RM, Pagel MD. Measuring Extracellular pH in a Lung Fibrosis Model with acidoCEST MRI. Molec Imaging Biol. 2015; 17:177–184. [PubMed: 25187227]
30. Chen LQ, Randtke EA, Jones KM, Moon BF, Howison CM, Pagel MD. Evaluations of tumor acidosis within in vivo tumor models using parametric maps generated with acidoCEST MRI. Mol Imaging Biol. 2015; 17:488–496. [PubMed: 25622809]
31. Moon BF, Jones KM, Chen LQ, Liu P, Randtke EA, Howison CM, Pagel MD. A comparison of iopromide and iopamidol, two acidoCEST MRI contrast media that measure tumor extracellular pH. Contrast Media Molec I. 2015; 10:446–455.
32. Fersht AR, Kirby AJ. Hydrolysis of aspirin. Intramolecular general base catalysis of ester hydrolysis. J Am Chem Soc. 1967; 89:4857–4863. [PubMed: 6074803]
33. Warburg O. On the origin of cancer cells. Science. 1956; 123:309–314. [PubMed: 13298683]
34. Vander Heiden MG, Cantley LC, Thompson CB. Understanding the Warburg effect: the metabolic requirements of cell proliferation. Science. 2009; 324:1029–1033. [PubMed: 19460998]
35. Sheth VR, Liu G, Li Y, Pagel MD. Improved pH measurements with a single PARACEST MRI contrast agent. Contrast Media Molec I. 2012; 7:26–34.
36. Ali MM, Yoo B, Pagel MD. Tracking the relative in vivo pharmacokinetics of nanoparticles with PARACEST MRI. Molec Pharmaceutics. 2009; 6:1409–1416.

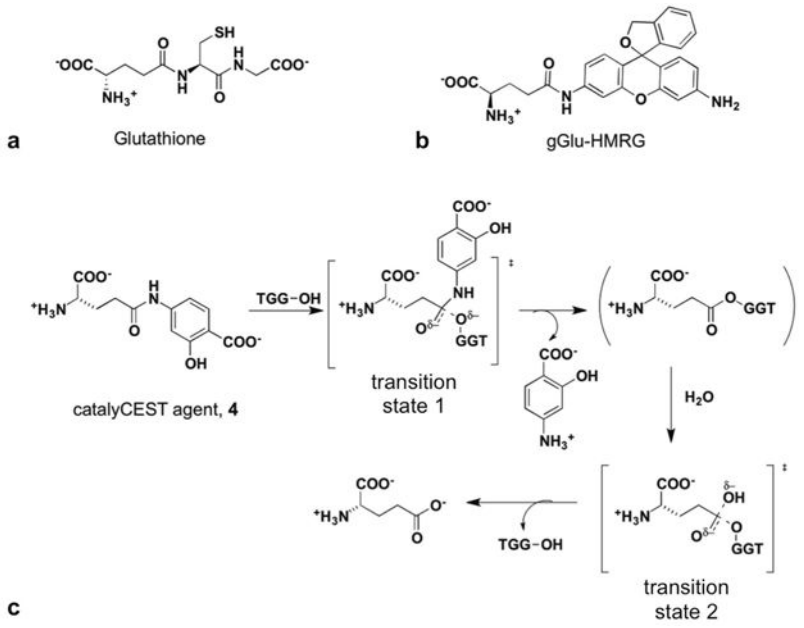

Figure 1.

Substrates for γ-glutamyl transferase (GGT). (a) The natural metabolite glutathione is cleaved by GGT to produce glutamate and a cysteine-glycine dipeptide. (b) A florescence agent, gGlu-HMRG, is activated after the glutamyl ligand is cleaved via GGT catalysis. (c) The proposed mechanism for GGT cleavage of the CEST MRI contrast agent, based on reference 16.

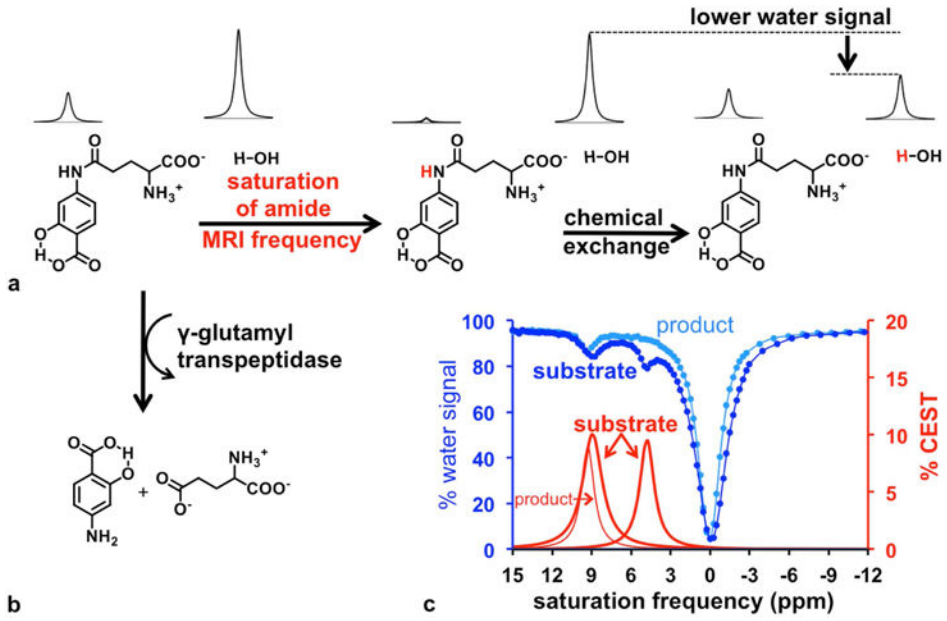

Figure 2.

CatalyCEST MRI. (a) Selective saturation of the net coherent magnetization of the amide proton (red hydrogen atom) followed by chemical exchange of the proton to water, causes a decrease in the MR signal of water. (b) The GGT enzyme can cleave the glutamyl moiety of the CEST agent, causing a loss of CEST signal from the aryl amide proton. However, the salicylic acid moiety can still generate a CEST signal. (c) The CEST spectra of the agent before and 12 hours after addition of GGT enzyme showed a disappearance of the CEST signal at 4.8 ppm while the CEST signal at 9.2 ppm was unchanged. Dark blue: CEST spectrum of the substrate; light blue: CEST spectrum of the product; Thick red line: % CEST signals of the substrate; thin red line: % CEST signals of the product.

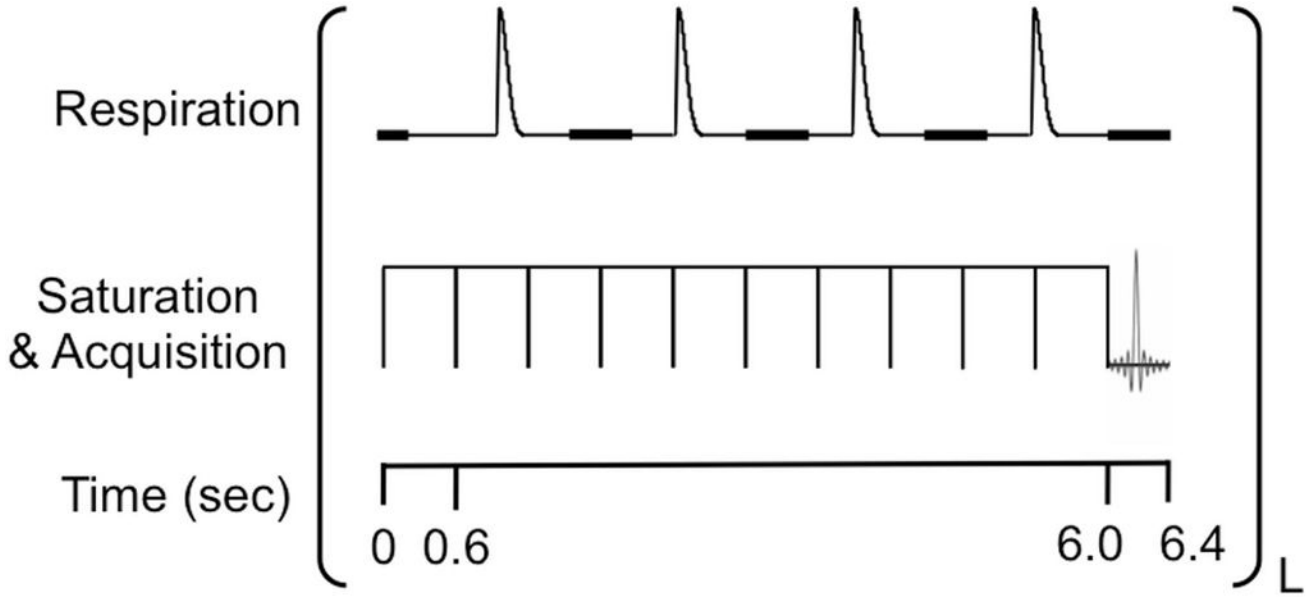

Figure 3.

The CEST-FISP MRI pulse sequence with respiration gating.[26] The respiration gating was adjusted to allow the start of acquisition in a 200 ms window (thick black line) that started 300 ms after inhalation. The series of saturation pulses typically ended within a respiration gating window, and the FISP acquisition was immediately started. Due to variable breathing rate, additional 600 ms saturation pulses was added to the saturation period until the total saturation period ended within a respiration gating window.

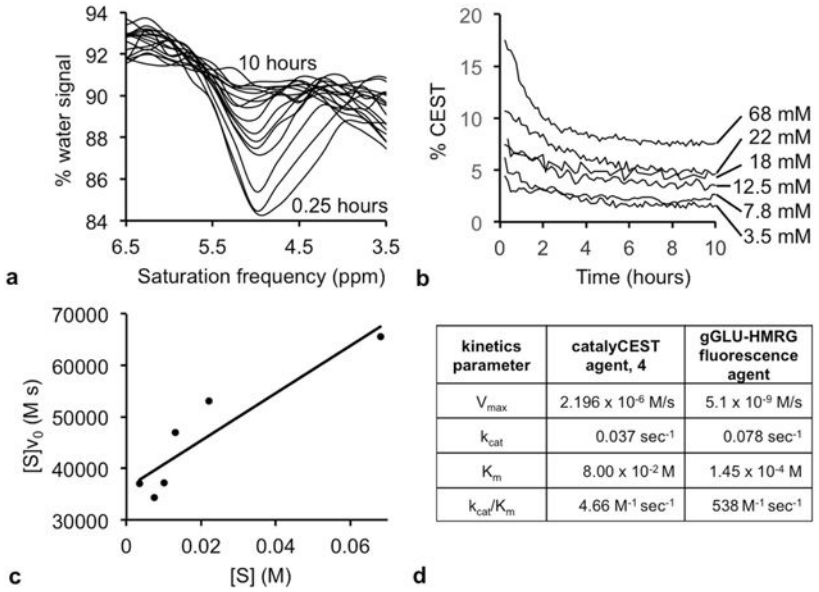

kinetics parameter	catalyCEST agent, 4	gGLU-HMRG fluorescence agent
V_{max}	2.196 x 10^{-6} M/s	5.1 x 10^{-9} M/s
k_{cat}	0.037 sec^{-1}	0.078 sec^{-1}
K_m	8.00 x 10^{-2} M	1.45 x 10^{-4} M
k_{cat}/K_m	4.66 M^{-1} sec^{-1}	538 M^{-1} sec^{-1}

Figure 4.

Michaelis-Menten enzyme kinetics. (a) The CEST spectrum showed a loss of the CEST at 4.8 ppm from 0.25 hours to 10 hours after adding enzyme to a 68 mM sample of the agent. (b) The % CEST at 4.8 ppm decreased when 0.4 units of GGT enzyme was added to each sample of the agent at different concentrations. The signal values were converted to concentrations (using the calibration shown in Sup. Fig. S4), and the initial reaction velocity, v_0, was determined from the loss in concentration during the first 2.5 hours after adding GGT enzyme to each sample. (c) A Hanes-Woolf plot was used to determine Michaelis-Menten kinetics parameters. (d) The k_{cat} rate of catalysis of the catalyCEST agent was comparable to the catalysis rate of a fluorescence agent. However, the K_M dissociation constant was higher for the catalyCEST agent, leading to a lower k_{cat}/K_M catalytic efficiency for the catalyCEST agent.

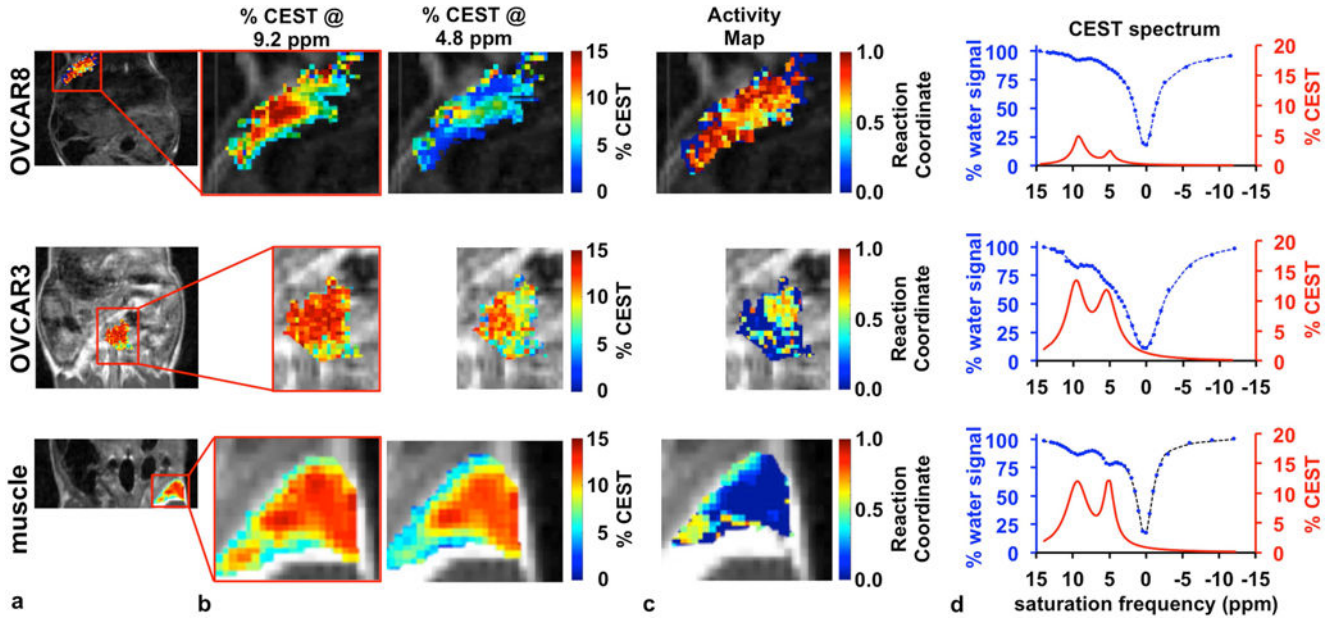

Figure 5.

In vivo catalyCEST MRI. (a) The anatomical images show the region of the OVCAR-8 tumor, OVCAR-3 tumor, and muscle tissue that was analyzed. The red rectangle shows the regions displayed in the remainder of the figure. (b) The parametric maps of % CEST signal amplitudes for CEST signals at 9.2 and 4.8 ppm demonstrate good detection of both CEST effects in the tumor and muscle tissues. (c) The activity maps of the GGT enzyme show high activity in the OVCAR-8 tumor, low activity in the OVCAR-3 tumor, and no activity in the muscle tissue. (d) The CEST spectra (blue) and CEST signals (red) for the region of the tumor and muscle also show good detection sensitivity of the agent and demonstrate the relative ratios of both CEST signals.

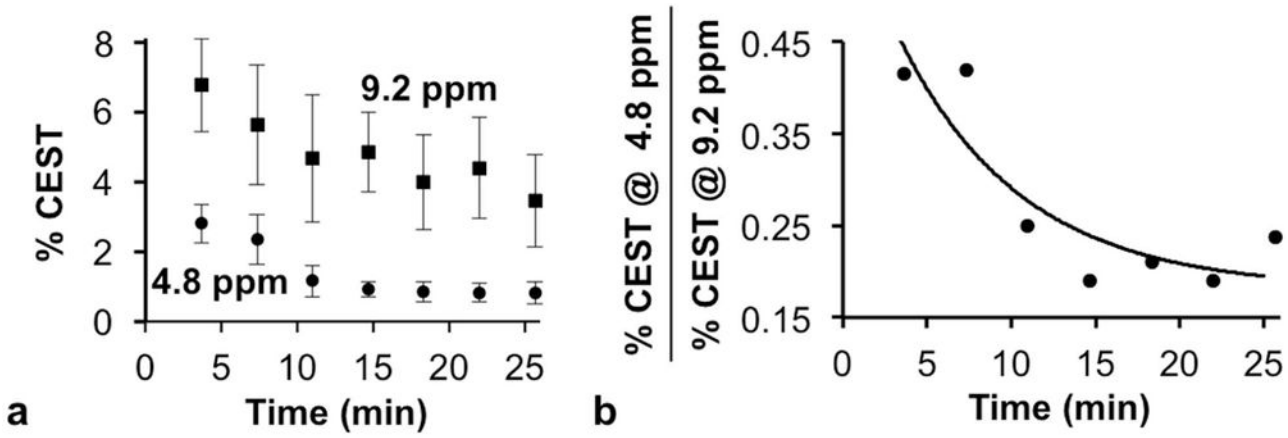

Figure 6.

Temporal catalyCEST MRI results. (a) The two CEST signals of the agent changed during the time course of the *in vivo* study, demonstrating that the agent experienced pharmacokinetic wash-out from the tumor as well as experiencing the effects of enzyme activity. Error bars represent the standard deviation of the measurements. (b) The temporal change of the ratio of the two CEST signals approximated a pseudo-first order reaction, as expected for enzyme kinetics with a high substrate concentration.

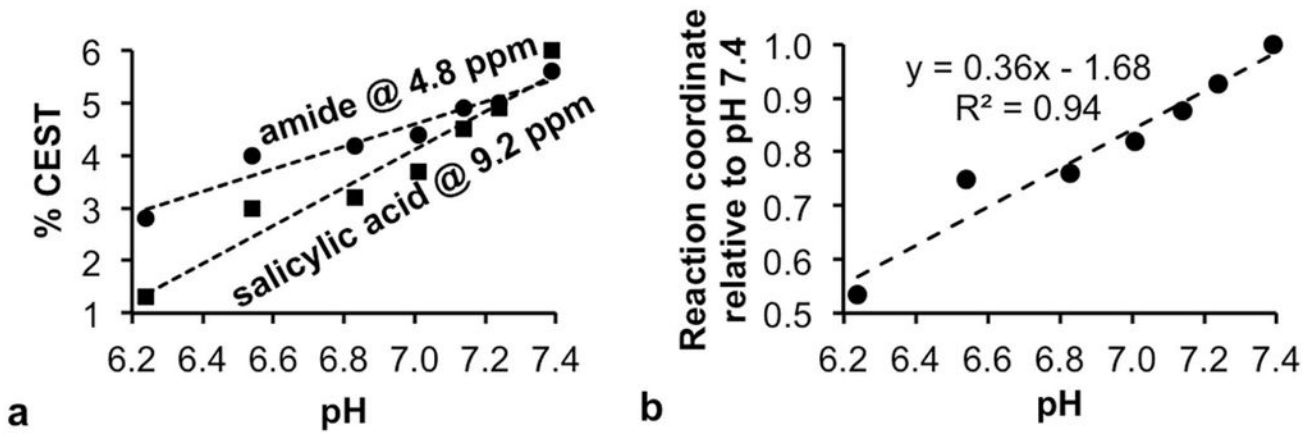

Figure 7.

The effect of pH on the determination of the reaction coordinate. (a) The chemical exchange rate of the salicylic acid moiety and aryl amide moiety are each base catalyzed, and therefore generate higher % CEST signal amplitudes at higher pH. (b) The % CEST signal amplitudes were converted to concentrations, then used to estimate a reaction coordinate at each pH value, which were normalized to the reaction coordinate at pH 7.4. Linear trendlines were fit to data in each graph. These results demonstrate that the reaction coordinate is underestimated under acidic pH conditions, which can occur in tumor tissues.

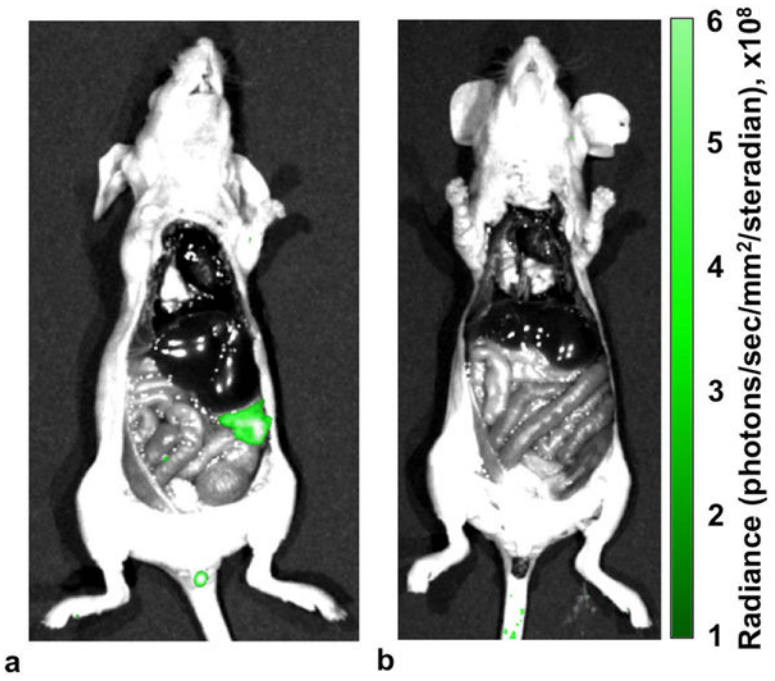

Figure 8.

Ex vivo fluorescence imaging with gGLU-HMRG dye confirmed that (a) the OVCAR-8 tumor had high GGT activity, (b) the OVCAR-3 tumor had GGT activity, and normal tissues had no detectable GGT activity.